https://doi.org/10.5194/egusphere-2024-454
Preprint. Discussion started: 28 February 2024

Measurement report: In-flight and ground-based measurements of nitrogen oxide emissions from latest generation jet engines and 100% sustainable aviation fuel

Theresa Harlass[1], Rebecca Dischl[1,2], Stefan Kaufmann[1], Raphael Märkl[1,2], Daniel Sauer[1], Monika Scheibe[1], Paul Stock[1], Tiziana Bräuer[1,2], Andreas Dörnbrack[1], Anke Roiger[1], Hans Schlager[1], Ulrich Schumann[1], Tobias Schripp[3], Tobias Grein[3], Linda Bondorf[3], Charles Renard[4], Maxime Gauthier[4], Mark Johnson[5], Darren Luff[5], Paul Madden[5], Peter Swann[5], Denise Ahrens[6], Reetu Sallinen[7] and Christiane Voigt[1,2]

[1] Deutsches Zentrum für Luft- und Raumfahrt, Institut für Physik der Atmosphäre, Oberpfaffenhofen, Germany
[2] Johannes Gutenberg-Universität Mainz, Institut für Physik der Atmosphäre, Mainz, Germany
[3] Deutsches Zentrum für Luft- und Raumfahrt, Institut für Verbrennungstechnik, Stuttgart, Germany
[4] Airbus Operations SAS, Toulouse, France
[5] Rolls-Royce plc. Derby, UK
[6] Rolls-Royce Deutschland, Dahlewitz, Germany
[7] Neste Corporation, Innovation, Porvoo, Finland

Correspondence to: Tiziana Bräuer (Tiziana.braeuer@dlr.de), Anke Roiger (Anke.Roiger@dlr.de)

Abstract. Nitrogen oxides, emitted from air traffic, are of concern due to their impact on climate by changing atmospheric ozone and methane levels. Using the DLR research aircraft Falcon, total reactive nitrogen (NO_y) measurements were carried out at high altitudes to characterize emissions in the fresh aircraft exhaust from the latest generation Rolls-Royce Trent XWB-84 engine aboard the long-range Airbus A350-941 aircraft. The impact of different engine thrust settings, monitored in terms of combustor inlet temperature, pressure, and engine fuel flow, was tested for two different fuel types: Jet A-1 and for the first time a 100% sustainable aviation fuel (SAF) under similar atmospheric conditions. During ground emission measurements, a range of combustor temperatures and an additional blended SAF were tested. We confirm that the NO_x emission index increases with increasing combustion temperature, pressure and fuel flow. We find that as expected, the fuel type has no measurable effect on the NO_x emission index. These measurements are used to compare to cruise NO_x emission index estimates from three engine emission models. Our measurements thus help to understand the ground to cruise correlation of current emission models while serving as input for climate modelling, and extending the extremely sparse data set on in-flight aircraft NO_x emissions to newer engine generations.

https://doi.org/10.5194/egusphere-2024-454
Preprint. Discussion started: 28 February 2024

1 Introduction

Aviation is a steadily growing transport sector (Lee et al., 2021), even despite the short-term drop during the COVID-19 pandemic (Le Quéré et al., 2020; Schumann et al., 2021; Voigt et al., 2022). As a result, emissions from air traffic are also expected to increase continuously and higher aircraft and engine efficiencies are surpassed by the overall air traffic growth. The exhaust of an aircraft engine burning conventional kerosene is constituted on average of ~3.16 kg carbon dioxide (CO_2) and ~1.23 kg water vapour (H_2O) per kg of fuel burned (Lee et al., 2021). Further emissions depend on the engine type, power settings, combustor technology and fuel composition and include nitrogen oxides (NO_x) as the sum of nitric oxide (NO) and nitrogen dioxide (NO_2), carbon monoxide (CO), unburnt hydrocarbons (C_xH_y), sulphur dioxide (SO_2) and soot (or non-volatile particulate matter, nvPM).

Most recent estimates (Lee et al., 2021) state that aviation since its historical beginnings contributes with +100.9 (55-145) mW m^{-2} to about 4 to 5% to total anthropogenic effective radiative forcing (ERF) (Grewe et al., 2019; Lee et al., 2021). Thus, air traffic emissions have a warming effect on climate. Contrail cirrus hereby represent the largest share of aviation ERF with ~57%, followed by CO_2 (~34%) and NO_x emissions (~17%; (Lee et al., 2021)). NO_x emissions from aviation contribute indirectly to anthropogenic ERF via a short-term warming and a long-term cooling effect (Brasseur et al., 1996; IPCC, 1999; Köhler et al., 2008; Lee et al., 2010; Dahlmann et al., 2011; Grewe et al., 2019; IPCC, 2021; Lee et al., 2021; Skowron et al., 2021; Terrenoire et al., 2022). The net ERF from NO_x, in sum, is however positive with 17.5 (0.6/29) mW m^{-2} (Lee et al., 2021). Other studies indicate that the contribution of NO_x in aviation ERF may be even higher due to simplifications in the methodology of previous estimates (Grewe et al., 2019). In the future, aviation NO_x emissions may have a net negative ERF, as the effect of emission of aircraft NO_x depends strongly on background emissions (Skowron et al., 2021).

Up to now, there is a lack of experimental measurements of NO_x emissions at cruise altitudes from state-of-the-art jet engines. Thus, in the joint ECLIF3 (Emission and CLimate Impact of alternative Fuels 3) project, direct (NO_x, CO, nvPM, H_2O) and indirect aircraft emissions (ice particles, vPM) were measured at high altitudes to understand and assess the impact of modern air traffic on the atmosphere, see also Märkl et al. (2023) and previous related projects as in Voigt et al. (2021). In this paper, we present a comprehensive set of NO_y emission measurements performed in the exhaust of the Airbus A350-941 with Rolls-Royce Trent XWB-84 engines. We derive emission indices from airborne measurements and compare them to ground-based measurements and three different engine emission prediction methods. We further investigate the effect of the Airbus aircraft burning 100% sustainable aviation fuel (SAF). Replacing conventional kerosene with SAF is one promising approach to reduce engine soot emissions, ice crystal number concentrations in contrails and the related climate impact, all in addition to a potential reduction of the CO_2 footprint in the life cycle analysis (Voigt et al., 2011; Moore et al., 2017; Kleine et al., 2018; Bräuer et al., 2021b; Bräuer et al., 2021a; Voigt et al., 2021).

https://doi.org/10.5194/egusphere-2024-454
Preprint. Discussion started: 28 February 2024

2 Materials and Methods

2.1 NO_x and CO_2 measurements

The DLR-operated research aircraft Falcon (reg. D-CMET, Dassault Falcon 20-E5), a twin-engine jet, was used as the airborne measurement platform. The in situ instrumentation consisted of several cabin-mounted trace gas (NO_y, CO, CO_2, H_2O) and aerosol instruments with their sample inlets located on the upper fuselage, see Figure 1b. Also, cloud particle probes were mounted in underwing pods to measure ice particle number concentrations and size distributions in ambient conditions (Märkl et al., 2023). Here, we focus on the NO_y and CO_2 measurement instruments as they are needed to derive the respective NO_x emission indices.

A well-established technique for measuring reactive nitrogen species, as employed in the present paper, includes their catalytic conversion to NO and subsequent detection using chemiluminescence technique. In general, chemiluminescence detectors (CLD) are widely used in atmospheric monitoring because they are sensitive with a detection limit as low as a few parts per trillion (ppt). In CLD, a sample of air passes through a reactor where NO is excited to NO_2^* by the reaction with high concentrations of O_3 produced by an ozone generator (Ridley and Howlett, 1974; Drummond et al., 1985). When returning to its ground state, the light emitted by the chemiluminescence reaction is proportional to the concentration of NO in the sample. By using selective converters directly upstream of the measurement chamber different reactive nitrogen species are converted to NO and subsequently detected by the CLD (Bollinger et al., 1983; Fahey et al., 1985). Within DLR, different types of CLD detectors have been used for atmospheric background measurements (Schlager et al., 1997; Ziereis et al., 2000; Schmitt, 2003; Stratmann et al., 2016; Ziereis et al., 2022) as well as in-plume detections (Schulte and Schlager, 1996; Schlager et al., 1997; Roiger et al., 2015). Aboard the Falcon a heated gold converter (T = 290 °C) with hydrogen (H_2) as reducing agent catalytically reduces all NO_y compounds to NO. NO_y is the sum of NO_x and all reactive nitrogen species as e.g. nitric acid, peroxyacetylnitrate (PAN) etc. The time resolution of the instrument is ~1 Hz with a detection limit of ~0.5 ppb. Under normal operating conditions the detector runs into saturation above mixing ratios of ~1000 ppb or ~1e6 counts per seconds. In order to measure at higher concentrations as expected in the exhaust plumes, a dilution system was integrated supplying zero air to the sample air in a ratio of 1/1 prior to the measurement. The NO_y measurement accuracy ranges between ~5 ppb near the detection limit and ~490 ppb at highest detected mixing ratios of ~4 ppm. It includes the following uncertainty parameters typical for CLD instruments, for details see (Stratmann, 2013): the sensitivity of the instrument (841 ± 95 counts/ppb), the efficiency of the NO_y converter (98.7 ± 1.5% at low and ± 30% at high concentrations), the instrumental interferences due to desorption processes and dark current (36 ± 118 counts), the statistical uncertainty of count rates (150-1600 counts), the uncertainty in the calibration standard (1% as stated by the manufacturer), the uncertainty due to the dilution system (7-21%) and due to a second instrument stage above 1e6 counts per seconds (i.e. 300 ppb).

A high frequency (~10 Hz) non-dispersive infrared gas analyser (LI-7000, LI-COR Biosciences) was used aboard the Falcon for in-plume CO_2 detections to be able to capture the small-scale variability of the plume. The LI-7000, uniquely modified in-house for aircraft deployment, uses two measurement chambers to detect CO_2: one is constantly flushed with dry zero air, the

https://doi.org/10.5194/egusphere-2024-454
Preprint. Discussion started: 28 February 2024

other is supplied with ambient air. The difference in absorption of infrared radiation passing through both cells is used to determine the absolute absorption and the absolute CO_2 mixing ratio (LI-COR, 2007). In the post processing, the CO_2 mixing ratio is corrected for dilution effects (LI-COR, 2003) and reported as dry air mole fraction. The CO_2 accuracy of the LI-7000 is independent with respect to the measured mixing ratios and is around 0.2 ppm. This includes the reproducibility of the calibration standards (0.08 ppm), the precision (0.08 ppm) and the uncertainty of water vapour measurement and thus the dilution correction (0.16 ppm). An occurring trend of the instrument response with instrument temperature and time is compensated by frequent zero measurements every 30 minutes during the flight. Absolute CO_2 mixing ratios and background values were cross checked with a second instrument aboard the Falcon, a cavity ring-down spectrometer (CRDS, Picarro G2401-m), due to its stable instrument performance (Fiehn et al., 2020; Klausner et al., 2020; Klausner, 2020).

Airborne measurements are complemented by in-field ground measurements. The CO_2 concentration was monitored via a LI-7200RS (LI-COR Biosciences) and the nitrogen oxide concentration was monitored via a CLD64 (ecophysics) chemiluminescence monitor. Both instruments were calibrated with certified calibration gases before each test run.

2.2 Emission sampling strategy

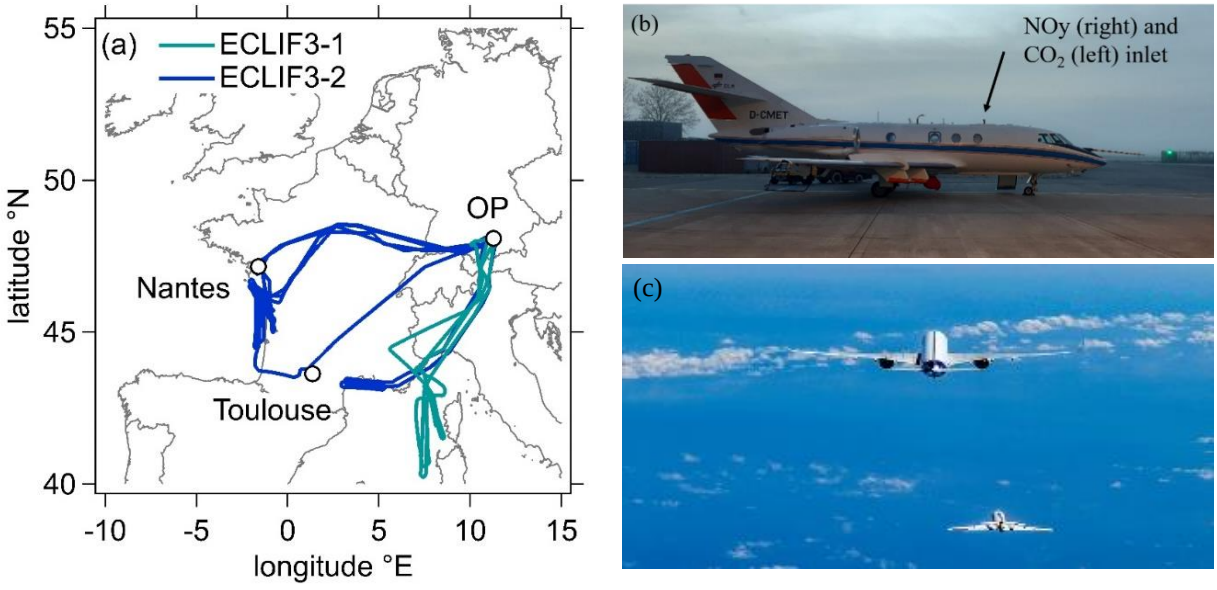

Figure 1: (a) Map of the Falcon flight routes, (b) inlet positions for trace gas sampling aboard the Falcon and (c) Falcon aircraft catching up to the Airbus A350 to perform emission measurements, © Airbus 2021, photo by S. Ramadier.

In-flight measurements at high altitudes were carried out under the framework of ECLIF3 in April 2021 (referred to as ECLIF3-1) and in November of 2021 (referred to as ECLIF3-2). This joint project was led by DLR and Airbus with Rolls-Royce, Neste, the University of Manchester and the National Research Council Canada (NRC) as partners. The objective of these flight campaigns was to characterize emissions behind an Airbus A350-941 (reg. F-WXWB) with Rolls-Royce Trent XWB-84 engines (ECLIF3-1: engine number 21004, ECLIF3-2: engine number 21012). This twin-engine aircraft is used for long-range

https://doi.org/10.5194/egusphere-2024-454
Preprint. Discussion started: 28 February 2024

distances by many operators since it is more fuel efficient than a four-engine long-range aircraft and older two-engine aircraft. During the mission flights, the Airbus aircraft was able to feed the engines from separate fuel tanks. Hence, measurements with two different fuels could be performed within single measurement flights which allowed probing of emissions at similar atmospheric conditions. As reference fuel, conventional Jet A-1 was used and provided by the local fuel supplier TotalEnergies. As sustainable aviation fuel, a 100% HEFA-SPK (Hydroprocessed Esters and Fatty Acids Synthetic Paraffinic Kerosene) made from sustainably sourced renewable waste and residues such as used cooking oil and other waste fat was provided by the project partner Neste.

Emission measurements were performed as close as possible to the Airbus aircraft at distances between 65 to 470 m (mean of 260 m), resulting in young plume ages of 0.3 to 3.5 s (mean of 0.8 s) in order to sample the fresh emissions before they undergo chemical processing in the atmosphere. Furthermore, it was aimed to study the emissions for various fuels at different combustor inlet parameters (temperature T3, pressure P3, engine fuel flow / fuel-to-air ratio) by varying the engine power settings and flight altitudes in defined but variable test point sequences. In total, six emission chase flights were performed along the western and southern French coast in temporary reserved air space, as shown in Figure 1a. The Falcon was mainly based in Oberpfaffenhofen (OP), Germany, and for a 5-day period in Toulouse, France, to minimize transfer flight times to the Airbus test area. With a take-off from OP, the Falcon had to be refueled in Nantes prior to the measurement flights along the Atlantic coast.

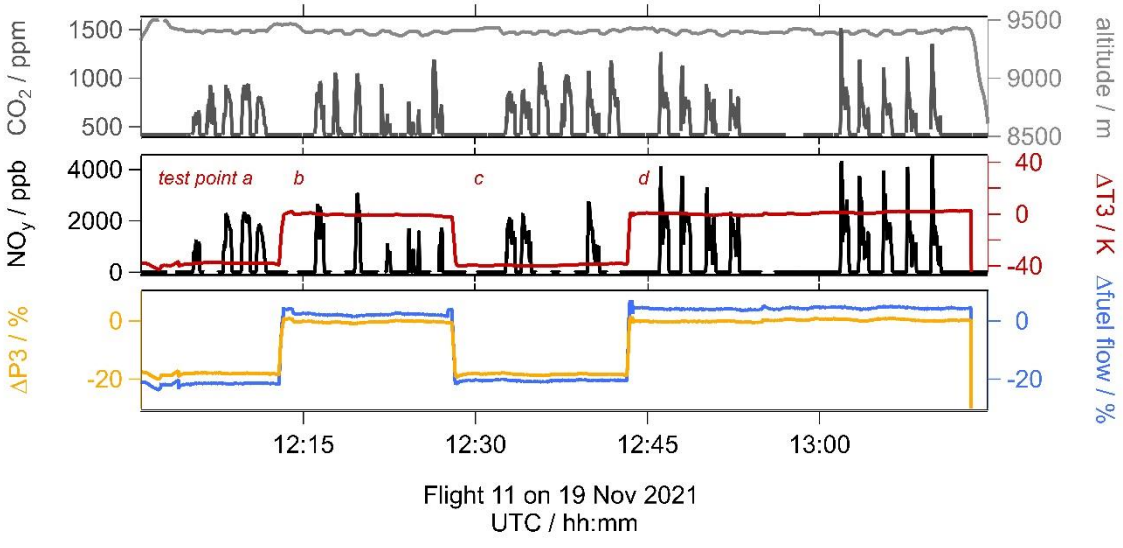

Figure 2: Emission measurement sampling sequence during the flight on 19 Nov 2021. Trace gases (CO_2, NO_y) and flight altitude as measured aboard the Falcon. Change in Airbus aircraft engine parameters (delta fuel flow, delta T3 temperature, delta P3 pressure) indicate different engine test points.

An example of an emission time series is shown in Figure 2. Measurements took place in the near field with the Falcon aircraft flying behind the Airbus aircraft under non- or only short-lived contrail-formation conditions. Usually, emissions were sampled from the right-hand side engine which was operated at different, well-defined cruise combustor inlet temperature conditions.

https://doi.org/10.5194/egusphere-2024-454
Preprint. Discussion started: 28 February 2024

The Falcon is the slower flying aircraft with a maximum cruise speed of ~200 m s^{-1}. To ensure that both aircraft speeds match in order to maintain the close distance, the Airbus aircraft had to adjust its speed by operating the left engine at a lower thrust. Hence, the test conditions probed in this study are not fully representative of typical cruise conditions. In addition, the Airbus aircraft also typically flies at higher altitudes (above FL350) compared to the altitudes which were sampled within this project (FL180 to 360). Generally speaking, this means that, at fixed T3 and DISA (Delta International Standard Atmosphere), the EIs measured at the lower test altitudes tend to be higher than the actual EIs at typical cruise altitudes (due to higher P3 at lower altitudes). Nevertheless, we assume that above FL300, this effect is small and the measurements can be directly compared to predictions at test conditions.

To ensure that the ceiling with the trace gas inlets is directly located in the exhaust plumes, the Falcon approached the exhaust trail from slightly lower altitudes. This position was held for ~50 s, then the Falcon dropped down to measure atmospheric background conditions for ~30 s. This alternating sequence was repeated 3-5 times for each test point with fixed engine parameters. Large enhancements (Δ) of CO_2 and NO_y were clearly visible with values typically between 100-800 ppm (ΔCO_2) and 500-4000 ppb (ΔNO_y) above mean atmospheric background values of 414-419 ppm and 0.6-4 ppb, respectively.

Ground measurements were performed in October 2021 in Toulouse, France. Sampling was performed with a stainless-steel probe at a height of 2.6 m and a distance of 24.5 m between the right-hand side engine exit plane and probe inlet. The exhaust was transported via a 40 m heated stainless-steel line to a manifold that allowed even distribution of air to the different measuring instruments.

2.3 Emission index calculation and plume definition

In order to quantify exhaust emissions from aircraft, the most common metric is the so-called emission index (EI), i.e. an emission quantity per mass of burned fuel. The NO_x emissions index (EI(NO_x)) is defined by convention in mass units of NO_2 (ICAO, 2008; Voigt et al., 2012; ICAO, 2023), hence the sum of NO and NO_2 in ambient air is calculated as if all NO was in the form of NO_2. Several studies discuss the composition of the different nitrogen species in the engine exhaust. E.g. (Kärcher et al., 1996; Tremmel et al., 1998; Bradshaw et al., 2000; Wormhoudt et al., 2007; Voigt et al., 2012) agree that at high engine power settings NO_x in the exhaust is dominated by NO (>80%). With growing plume age, the NO and NO_2 ratio is determined by an equilibrium of the reaction of NO and O_3, forming NO_2 and the photolysis of NO_2 (Tremmel et al., 1998). In addition, small amounts of HNO_2 and HNO_3 are formed in the ageing plume from the NO_x emissions. Hence, by measuring NO_y aboard the Falcon all reactive nitrogen species in the exhaust can be detected and related to the initial NO_x emissions. For each individual plume encounter EI(NO_x) is derived based on the inert dilution tracer CO_2 via Eq. (1) following Schulte et al. (1997):

$$\mathrm{EI}\,(\mathrm{NO}x) = \frac{\int \Delta NOy}{\int \Delta CO_2} * EI(CO_2) * \frac{M(NO_2)}{M(CO_2)}, \quad (1)$$

where $\int \Delta NOy$ and $\int \Delta CO_2$ is the integrated enhancement above an atmospheric background level; $EI(CO_2)$ is the emission index of CO_2 dependent on the fuel used (see Table 1); and $M(NO_2)$ and $M(CO_2)$ are the molar masses of NO_2 (46.0055 g mol^{-1}) and CO_2 (44.0095 g mol^{-1}).

https://doi.org/10.5194/egusphere-2024-454
Preprint. Discussion started: 28 February 2024

An individual plume encounter denotes a plume crossing in a time series where enhancements of NO_y and CO_2 start exceeding background level variations, denoting the plume beginning, and the subsequent return to atmospheric background level, denoting the plume end. Between plume beginning and end a minimum 7 second plume length threshold was chosen to exclude accidental plume encounters. Further plumes were rejected due to Airbus aircraft engine instability (e.g. variability of T3 greater than ± 2 K) and/or low correlation between CO_2 and NO_y measurements ($R<0.7$). The individual plume crossings of the background-corrected mixing ratios of each species are integrated over time (and hence, over the horizontal extent of the plume) to account for the inlet positions (about 30 cm difference in the horizontal direction), tubing lengths and different instrument response times. Due to the variable position of the Falcon aircraft within the turbulent exhaust plume and thus variable plume dilution values, it is necessary to normalize NO_y mixing ratios to the measured CO_2 concentration. CO_2 hereby acts as a chemically inert species to determine the dilution of the engine emissions at the measurement point. CO_2 emission indices are a fuel-dependent metric and are derived from the hydrogen and carbon content of the fuel under the assumption that it is completely burnt and all available carbon is converted to CO_2. The emission index $EI(CO_2)$ can then be calculated via Eq. (2) following Moore et al. (2017):

$$\mathrm{EI}\,(CO_2) = \frac{RT}{pV_m} * \frac{M(CO_2)}{M(C)+\alpha M(H)}, \quad (2)$$

where R is the ideal gas constant (8.31 J mol^{-1} K^{-1}); T and p are the temperature (273.15 K) and pressure (101325 Pa) at standard conditions; V_m is the molar volume at standard conditions (0.0224 m^3 mol^{-1}); $M(C)$ and $M(H)$ are the molar masses of carbon (12.01 g mol^{-1}) and hydrogen (1.01 g mol^{-1}); and α is the hydrogen-to-carbon molar ratio of the fuel (as calculated based on Table 1). As the batches of the fuel supplier varied between the two measurement campaigns, also the fuel properties slightly varied. Their characteristic hydrogen and carbon contents are listed in Table 1 together with the calculated emission index of CO_2. The hydrogen content was measured via low resolution nuclear magnetic resonance spectrometry (ASTM D3701 with a repeatability of 0.09% and reproducibility of 0.11%). The carbon content is assumed to add up to 100 mass% with the hydrogen content and sulphur content (not listed), and was cross checked via ASTM D5291 (which has a repeatability of 0.94% and reproducibility of 2.42%).

Table 1: Hydrogen and carbon content of Jet A-1 and HEFA-SPK during the two airborne measurement projects. $EI(CO_2)$ is estimated following Moore et al. (2017). For the ground measurements also the HEFA-SPK blend is listed.

Project	Fuel type	Hydrogen content / mass%	Carbon content / mass%	$EI(CO_2)$ / g kg^{-1}
ECLIF3-1	Jet A-1	14.08	85.90	3149
	HEFA-SPK	15.11	84.89	3111
ECLIF3-2 (ground and flight)	Jet A-1	14.25	85.74	3142
	HEFA-SPK	15.18	84.82	3108
	HEFA-SPK blend	14.39	85.56	3137

https://doi.org/10.5194/egusphere-2024-454
Preprint. Discussion started: 28 February 2024

2.4 ICAO Aircraft Engine Emissions Databank

The reporting of emissions in the vicinity of airports is mandatory for engine manufacturers during certification processes for individual engine types and reports are voluntarily made publicly available at the International Civil Aviation Organization (ICAO) Aircraft Engine Emissions Databank (EEDB). For that, a landing and takeoff (LTO) cycle is defined to derive emissions during taxi-out/taxi-in, approach, climb and takeoff in a consistent manner (ICAO, 2008). While varying the engine power settings, and thus the fuel flow rate at a test stand, emissions at sea level conditions are measured. Thrust levels of 7%, 30%, 85% and 100% hereby correspond to taxi-in/taxi-out, approach, climb and takeoff conditions.

As NO_x emissions highly depend on temperature and pressure in the engine combustor, they are derived for different thrust settings related to different flight phases at certification ground test for International Standard Atmosphere (ISA) conditions. In general, NO_x emissions increase with increasing power and increasing fuel flow, see Figure 3. Thermal NO formation, first described by Zeldovich in 1946 and therefore also referred to as Zeldovich mechanism, is one of the main sources of nitrogen oxides in combustion dominating at high pressure and temperature conditions typical for a jet engine (Lavoie et al., 1970). However, as chemical equilibrium of the thermal NO formation route is not reached within typical timescales of a combustor, total formed NO_x in a modern rich burn combustor is strongly dependent on the quick quenching and mixing of the hot streams of the primary combustion zone. Combustor design optimised for NO_x emissions aims for enhanced mixing and reducing residence time in areas of high temperature. For a given combustor design, NO_x emissions depend on operating conditions as pressure temperature and local air-to-fuel ratio in the combustor. NO_x in a gas turbine combustor, i.e. at high pressure and temperature, is predominantly formed via thermal NO pathway. Thermal NO_x formation rate increases exponentially with temperature and further depends on pressure (Gokulakrishnan and Klassen, 2013). In comparison to all ~560 engine types covered by the EEDB (depicted in grayish/black; (EEDB, 2021)), NO_x emissions from the Rolls-Royce Trent XWB-84 engine (depicted in blue) are rather at the upper limit when considering the thrust settings, but typical for a modern large engine powering the long range planes. This engine is specifically designed for a modern long-range aircraft being the most fuel-efficient large aero-engine in revenue service, and therefore it operates at high pressure ratios and combustor exit temperatures to deliver the required thrust at high fuel efficiency. Therefore, NO_x emissions tend to be higher than for engines operating at lower overall pressure ratio (OPR).

https://doi.org/10.5194/egusphere-2024-454
Preprint. Discussion started: 28 February 2024

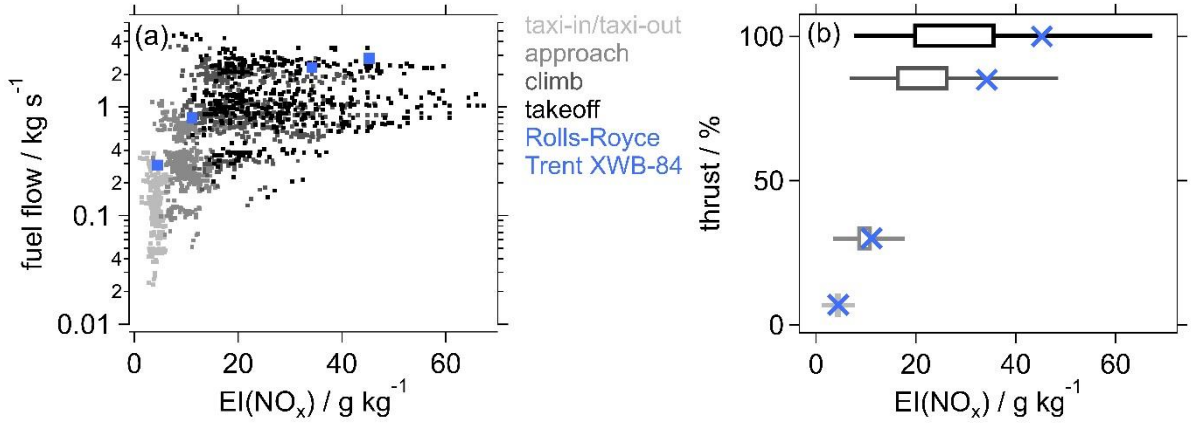

Figure 3: EI(NO_x) based on the entire ICAO Aircraft Engine Emissions Databank v28B (EEDB, 2021). Panel (a) shows the dependency on fuel flow, panel (b) on thrust. The Rolls-Royce Trent XWB-84 engine, which was the focus during ECLIF3, is highlighted in blue.

The certification engine emission data cover a standardised LTO cycle intended to cover local air quality. To predict EIs of the whole flight envelope, different modelling approaches exist, which use ground test data and correct them to atmospheric conditions at the respective flight level, flight phase and engine thrust setting, as e.g. done when applying the Rolls- Royce model or Fuel Flow correlation methods as described in the next section.

2.5 P3T3 and Fuel Flow methods

Based on the set of emissions data determined during the engine certification process, one can derive emission indices over various flight profiles using engine performance and emission models. A modern high-bypass turbofan engine in general follows a Brayton or Joule Cycle, where, after a fan, two air streams are separated: in the core of the engine, pressurized air and fuel are burned (temperature is increased by the heat release in the combustion chamber), and passed through a turbine, and together with the larger bypass air, propulsion thrust is produced. The subsequent positions are characterized and defined by total temperature and pressure regions: T2/P2 at the fan inlet, T24/P24 at the low-pressure compressor outlet, T3/P3 at the high-pressure compressor outlet and T5/P5 at the low-pressure turbine outlet. However, input data such as e.g. P3 and T3 are proprietary and thus not publicly available.

Engine performance data or models can be used to directly predict emissions at altitude, which is called P3T3 method (DuBois and Paynter, 2006). Manufacturers thus have developed their own prediction methods for non-LTO conditions based on correlations derived from empirical rig data to correct for the effect of a change in combustor inlet pressure (P3) and combustor Air Fuel Ratio (AFR) at a fixed combustor inlet temperature (T3). These correlations are typically referred to as P3T3 methods as often the AFR exponent may be set to zero. However, as NO_x sensitivity to AFR depends on the stochiometric distribution within the combustion zones of a rich burn combustor, it may also be set to some small number to reflect more EI(NO_x) at

https://doi.org/10.5194/egusphere-2024-454
Preprint. Discussion started: 28 February 2024

richer AFRs (towards higher power), as done for this comparison where AFR is set to 0.5. The validation of these methods has proven to be accurate within 10%.

The EI NO_x must further be corrected to the lower pressure at altitude compared to sea-level static $(P3_{sealevel}/P3_{altitude})^y$. The exponent y is unique for every engine and derived by the manufacturers, but commonly ranges between 0.2 to 0.5 with typically 0.5 for a rich burn combustor being used. In addition, NO_x emissions are also dependent on the ambient humidity as the additional heat capacity of the water reduces combustion temperature, and thus the NO_x formation rate. Either actual humidity measurements are needed or a reference humidity of 60% is assumed (ISO 5878). In-flight measurements of relative humidity in the ECLIF3 test areas show values between 30 and 70%, hence the reference value is a reasonable assumption. However, this relative humidity at cold ambient temperature at altitude relates to a much lower absolute humidity by mas compared to ground reference condition of 6.34 g/kg. Based on the certification humidity correction formula for $EI(NO_x)$, cruise predictions must include a humidity correction of around +12%.

The direct P3T3 method requires proprietary engine data, which are not available for modelers. Simplified methods were developed to estimate NO_x emissions relating in flight fuel flow at altitude to publicly available fuel flow data and corresponding $EI(NO_x)$ in the ICAO emissions databank. Such fuel flow methods (FFM) provide corrections to the different flight conditions such as altitude, humidity and Mach number (Deidewig et al., 1996; Döpelheuer and Lecht, 1999; DuBois and Paynter, 2006). The ground-based values, as reported by the ICAO Aircraft Engine Emissions Databank, are logarithmically fitted with respect to fuel flow. For $EI(NO_x)$, a power function fit leading to linear relations in a log-log plot is used between two points. Previously published comparisons with in situ NO_x observations of older engines have shown that predictions based on fuel flow models and in-flight measurements agreed on average within ±12% (Schulte et al., 1997). For conventional rich burn combustors fuel flow methods like Boeing FFM2 (DuBois and Paynter, 2006) are able to predict altitude emissions within 10% compared to the full proprietary P3T3 method (Norman, 2003; SAE, 2009).

In this paper we use the calculated $EI(NO_x)$ of three different prediction methods and compare them to the in flight measurements: (a) the Boeing Fuel Flow Method2 (BFFM2) with which Rolls-Royce estimated $EI(NO_x)$ at the tested operating conditions; (b) a method based on the Fuel Flow Method2 (DuBois and Paynter, 2006) adapted and improved by DLR (aptFFM2) as described in Teoh et al. (2022); and (c) the Rolls-Royce in-house P3T3 method. For the fuel flow, actual observational data and the EI(CO2), according to Table 1, served as input. Differences between aptFFM2 and BFFM2 models are that the aptFFM2 method uses total pressure and temperature, therefore calculating the effect of aircraft speed, while the BFFM2 method uses ambient pressure and Mach number (Schaefer and Bartosch, 2013).

* as coded in December 2022 in python by Roger Teoh and Marc Stettler at Imperial College and converted in 2022 to Fortran by our team at DLR.

https://doi.org/10.5194/egusphere-2024-454
Preprint. Discussion started: 28 February 2024

3 Results and Discussion

In-flight measurements aboard the DLR research aircraft Falcon were carried out in the framework of the ECLIF project in 2021. Based on these in situ measurements at high altitudes we quantify exhaust emissions by inferring emission indices of NO_x valid for the young exhaust of a long-range A350-941 aircraft with latest generation Rolls-Royce Trent XWB-84 engines. For the first time, the Airbus aircraft was fuelled with 100% SAF (Airbus, 2021b, a; Rolls-Royce, 2021). The aircraft was able to switch between Jet A-1 and SAF during the flight mission, hence, the impact of fuel effects could be measured in comparable atmospheric conditions. Furthermore, different engine power settings, e.g. compressor exit temperatures and pressure, as well as engine fuel flows / fuel-to-air ratio, were studied at high altitudes. Due to the confidential nature of detailed aircraft and engine parameters, we do not relate the derived emission indices to absolute values of engine sensitive parameters, but use a delta notation (Δ) to a representative observed value of the flight mission.

3.1 In-flight NO_x emissions

The emitted NO_x of an aircraft engine is dependent on actual thrust and resulting combustor conditions as inlet temperature T3 and pressure P3, as well as local air-to-fuel ratio. Hence, we present EI(NO_x) values depending on different source engine parameters, as listed in Table 2.

Table 2: Normalisation of source engine parameters.

Abbreviation	Parameter	Unit	State within individual test points
ΔT3	total temperature at HPC exit relative change to a representative mission value	K	controlled adjustment
ΔP3	total pressure at HPC exit relative change to a representative mission value	%	changes with T3 adaptations
ΔFF	fuel flow rate per engine relative change to a representative mission value	%	changes with T3 adaptations
Mach	Mach number ratio of true air speed (TAS) and local speed of sound	-	constant
T2	Total temperature at fan intake	%	constant

Since the temperature at the exit of the high-pressure compressor (HPC), T3, is one of the major parameters affecting emissions, engine throttle was set in order to achieve various levels of T3 in the cruise range (low, mid and high-power cruise). This led to a different P3 and fuel flow levels, while Mach number and T2 were held roughly constant during different test points by adjusting the second engine.

https://doi.org/10.5194/egusphere-2024-454
Preprint. Discussion started: 28 February 2024

The dots in Figure 4a show emission indices derived from near field measurements on 19th of November 2021 at flight level (FL) 310 for varying ΔT3. Two different T3 settings and fuel types (Jet A-1 and 100% HEFA-SPK) were probed during that flight. The flight altitude (9465 ± 10 m), Mach number (0.62 ± 0.003) and T2 (± 1%) were held constant within the different test points, while T3 was increased by ~40 K. This led to a simultaneous increase in P3 by ~19% and fuel flow by ~26%. First, at ΔT3 of approx. -40 K the mean EI from Jet A-1 (16.2 ± 0.3 g kg-1) and HEFA-SPK (15.6 ± 0.2 g kg-1) agree within their error estimates. Hence, no statistically significant impact of fuel type on EI(NO_x) can be detected. This is within expectation, since it is assumed that the usage of different fuel types do not alter stochiometric distribution within the combustion chamber. Second, the mean EI for Jet A-1 increases over the T3 range by ~20% (to 19.1 ± 0.4 g kg-1), the mean EI for HEFA-SPK by ~17% (to 18.3 ± 1.7 g kg-1). Therefore, it can also be concluded that both fuels show similar sensitivities to combustion conditions as temperature and pressure as expected.

The squares in Figure 4a represent measurements on 14th and 16th of April 2021 at FL360 to underline the two observations above with additional measurement points on a different day and at different flight altitude. At the ΔT3 setting of approx. -15 K the mean EI(NO_x) for Jet A-1 and HEFA-SPK again are in agreement within expected uncertainties. HEFA-SPK, in addition, was probed at two higher T3 settings (approx. 0 K and approx. 15 K) and shows also an increasing trend in mean EI(NO_x) from 16.7 ± 0.5 to 18.4 ± 1 and 22.0 g kg-1.

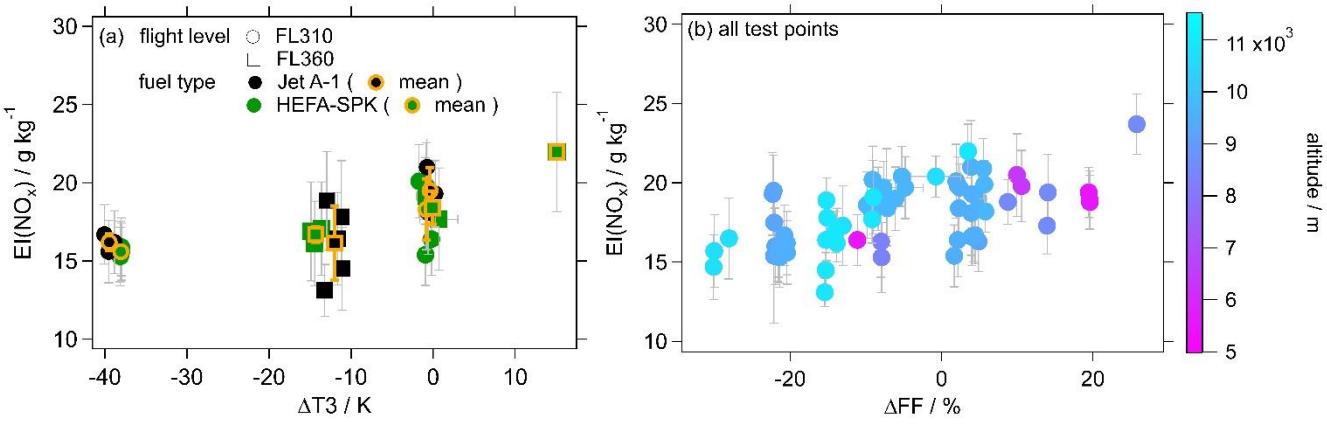

Figure 4: EI(NO_x) as calculated from in-flight measurements behind the A350 with Rolls-Royce Trent XWB-84 engines (a) versus ΔT3 at constant conditions at FL310 and FL360, (b) versus Δfuel flow; color coded by altitude for all acquired data points.

Figure 4b presents all data points acquired during the ECLIF3 campaign plotted against fuel flow range and color coded by flight altitude. Despite the scattered data, the expected increase in NO_x emissions with increasing fuel flow can be recognized. Due to the multi-dimensional dependency of EI(NO_x) on more than one engine parameter we cannot further assess the relative importance of individual engine parameter changes. However, we do not observe differences for the different flight altitudes where the measurements took place.

The spread of individual EIs in Figure 4a may be due to sensitivity of NO_x to ambient conditions. The standard deviations from the means in ΔT3 EIs on 19 November 2021 (dots) are between 3-8% for Jet A-1 and around 2-11% for HEFA-SPK.

https://doi.org/10.5194/egusphere-2024-454
Preprint. Discussion started: 28 February 2024

The standard deviations from the means for ΔT3 EIs on 14 and 16 April 2021 (squares) are up to 15 % for Jet A-1 and 3-6 % for HEFA-SPK. However, these internal variabilities are still smaller than the increasing trend of the mean values with T3.

3.2 Comparison with engine emission models

In this section we compare our near field in-flight measurements with model predictions. Please note that all ECLIF3-1 and -2 test points were analysed using BFFM2 and aptFFM2, whereas P3T3 model results are only available for ECLIF3-2. The model uncertainty for BFFM2 is around 10% for conventional rich burn (DuBois and Paynter, 2006), for aptFFM2 ~20% (ICAO, 2020; Teoh et al., 2022), for P3T3 around 10 to 15% (SAE, 2009) and for the observational EIs ~14% as derived from emission index uncertainty analysis below.

In general, the observation to model agreement is good with a correlation coefficient (R^2) of 0.3 to 0.4. For aptFFM2 / BFFM2 / P3T3 roughly 40 / 50 / 75 % of data points agree within a difference of ±3 g kg^{-1} and are thus well within the combined errors of model results and measurements. Deviations between the models are within the error limits. However, predicted EIs tend

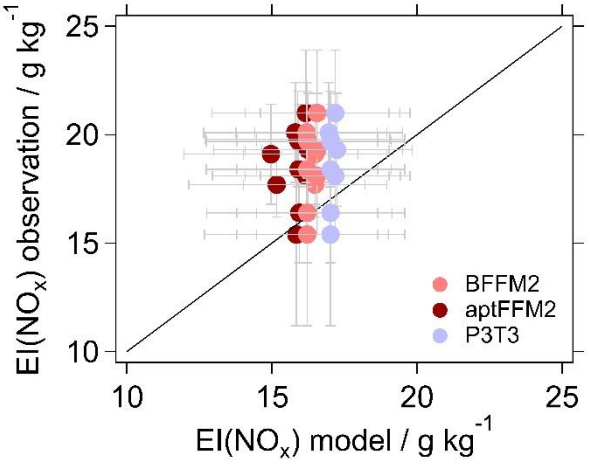

Figure 5: EI(NO_x) from observations and three model estimates for the 0 K ΔT3 setting at FL310 and FL360. The black line marks the 1:1 agreement.

to be on average ~15% (aptFFM2, P3T3) to ~20% (BFFM2) lower than calculated EIs from the in-flight measurements in near field conditions. Figure 5 shows, analogous to Figure 4a, only data points for constant flight conditions at FL310 and FL360 with a focus on the ΔT3 setting of 0 K. This subset focuses on a set of conditions for which the DISA was quite similar, hence the atmospheric temperature conditions do not affect the emission indices. Still, the model predictions tend to show smaller EIs than determined by the in-flight measurements of the engines at cruise at slightly lower Mach numbers compared to typical cruise conditions. In order to investigate in flight engine performance at typical cruise conditions we compare model predictions to far field measurements in the next section. Furthermore, to reduce effects of engine-to-engine variability we use ground measurements at the same engine instead of predictions from the data base.

https://doi.org/10.5194/egusphere-2024-454
Preprint. Discussion started: 28 February 2024

3.3 Ground-based NO_x emissions

The ground-based engine tests were performed on two days at similar ambient temperatures. The reference measurements with fossil Jet A-1 were performed on 22 October 2021 (temperature: 12.2°C - 14.4°C; relative humidity: 87% - 81% during test run). The neat HEFA-SPK and an additional SAF blend (HEFA-SPK blended with a different Jet A-1) were tested on 23 October 2021 (temperature: 9.1°C - 15.2°C; relative humidity: 47% - 96% during test run). The hydrogen and carbon content by mass% of the SAF blend are 14.39% and 85.61% respectively (see Table 1). Four test points with Jet A-1 were repeated on the second day in order to identify any biases from changes in environmental conditions or different probe alignment. The engine was operated at several different power settings ranging from idle conditions to maximum climb. Each test point was stabilised for a few minutes and after reaching a stable T3, sampling was performed for 5-6 minutes. In case of the highest thrust settings, the sampling time was reduced to 2-3 minutes. During the ground measurements a large T3 temperature range was covered. Thus, the ground measurements allow the detection of the $EI(NO_x)$ curve over a larger range of T3 and fuel flows.

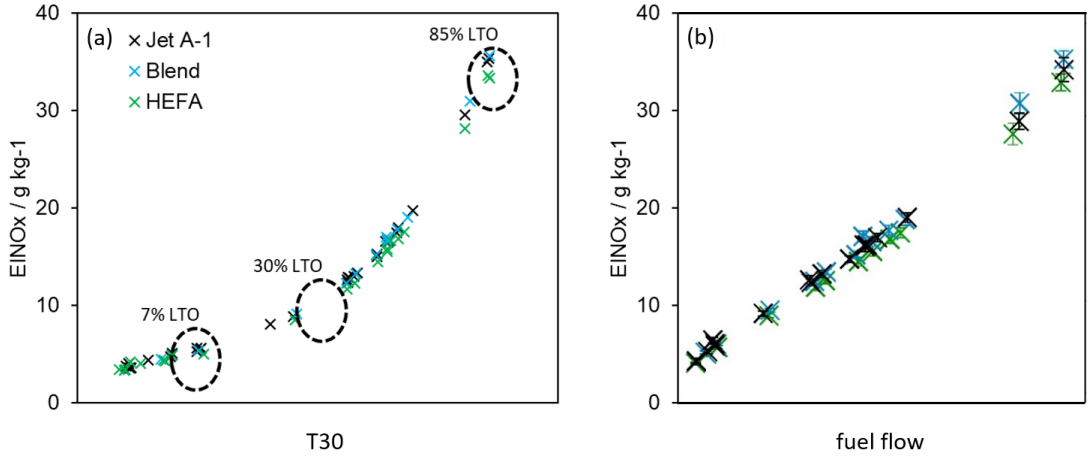

Figure 6: $EI(NO_x)$ from ground measurements behind the A350 with Rolls-Royce Trent XWB-84 engines versus desensitized T3 (referenced to 60% RH, (a)) and Δfuel flow (b) for Jet A-1, HEFA-SPK and Blend. Black circles indicate LTO points.

The NO_x emission curve shows a continuous increase with higher thrust, and corresponding increasing T3, P3 and fuel flow. These dependencies are recognizable from Figure 6, where NO_x is plotted over T3 and fuel flow. As expected and discussed above, NO_x emissions are not significantly affected by the fuel composition. The observed emission indices are within estimated error margins. These findings are in line with results of ground-based measurements behind an Airbus A320-232 with IAE V2527-A5 engines in 2018 using fossil Jet A-1 fuels as well as blends of HEFA-SPK and Jet A-1 as discussed by Schripp et al. (2022). They also found an independence of NO_x emissions on fuel type, and similar sensitivities to combustion temperature ($\Delta T3$ ~40K, $\Delta EI(NO_x)$ ~4 g kg^{-1}). Bulzan et al. (2010) also presented and discussed NO_x results of a ground-based campaign in 2009 targeting the CFM56-2C1 engine of the NASA DC-8 aircraft burning pure fossil fuels (JP-8) as well as

https://doi.org/10.5194/egusphere-2024-454
Preprint. Discussion started: 28 February 2024

blends with Fischer-Tropsch fuels based on natural gas and coal. They found an increase of EIs with fuel flow by about ~6 g kg^{-1} per ~100% more burned fuel, which is in line with the measurements performed in this study.

Figure 7 shows predictions using the ground measurements during the ECLIF3-2 campaign with the identical Rolls-Royce engine as input (see Figure 6) for engine emission model predictions to cruise altitudes and conditions. Although the lower absolute humidity should increase NO_x by 12%, in general, lower NO_x levels compared to the ground measurements are expected due to the lower pressure at altitude. The predictions are compared to far field measurements of the Falcon, obtained within the same project, but with both aircraft flying at typical cruise conditions and Mach numbers. The two engine models agree well with the measurements at cruise altitudes within the estimated uncertainties. The BFFM2 predictions are typically 10% higher compared to P3T3 methods which has been found before for this type of combustor, but are still within the ΔT3 ranges. The agreement between the models and the in flight measurements is significantly improved by using the ground based EI(NO_x) measurements on the same engine instead of using emission data from the engine emission data base used for Figure 5. The use of ground measurement data on the same engine takes into account a potential slight change in engine performance of well-maintained in operation engines. The comparison to in-flight measurements at typical cruise conditions in terms of T3, P3, AFR and Mach number also ensures a better comparability of the predictions well within the range tested in rig tests.

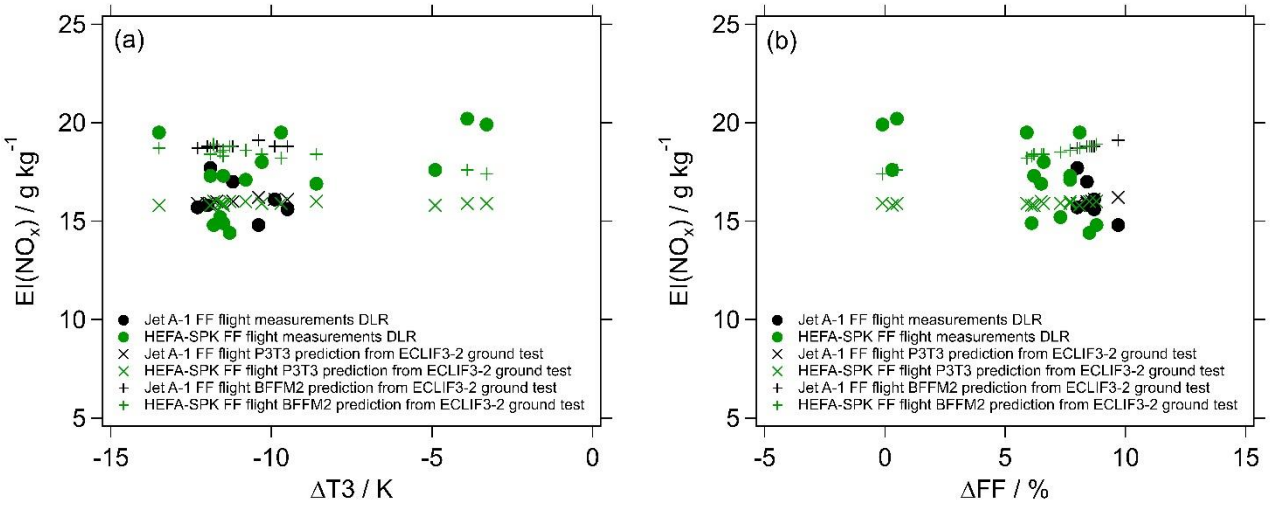

Figure 7: EI(NO_x) (dots) from in flight measurements for different fuels at typical cruise Mach numbers in the far field at flight level 320 and FL350 from ECLIF3-2 behind the A350 with Rolls-Royce Trent XWB-84 engines versus desensitized T3 (a) and desensitized fuel flow (b). Modelled EI(NO_x) for the far field measurement conditions from the P3T3 model (cross) and the Boeing Fuel Flow Method2 (plus) calculated based on ECLIF3 ground measurements shown in Figure 6.

3.4 In-flight emission index uncertainty analysis

Here, we present an in-depth analysis of different aspects contributing to the uncertainty of each individual inferred emission index (see Eq. (1)) with respect to the in-flight measurements. The EI uncertainty consists of several individual errors: (a) the uncertainty of the enhancement above an atmospheric background level ($\partial(\Delta NO_y)$ and $\partial(\Delta CO_2)$), which can be subdivided into (a.a) the absolute accuracy of the measured species (∂NO_{y_acc}, ∂CO_{2_acc}) and (a.b) the uncertainty related to the atmospheric

https://doi.org/10.5194/egusphere-2024-454
Preprint. Discussion started: 28 February 2024

background determination (∂NO_{y_bgr}, ∂CO_{2_bgr}); (b) the uncertainty in EI(CO_2); and (c) the uncertainty in the molar masses of NO_2 and CO_2. The total uncertainty (∂) is then estimated using Gaussian error propagation following Eq. (3):

$$\partial \mathrm{EI(NO}x) = \pm \sqrt{\begin{aligned}&\left(\frac{\partial \mathrm{EI(NO}x)}{\partial NOy}\partial NO_{y\_acc}\right)^2 + \left(\frac{\partial \mathrm{EI(NO}x)}{\partial NOy}\partial NO_{y\_bgr}\right)^2 + \left(\frac{\partial \mathrm{EI(NO}x)}{\partial CO_2}\partial CO_{2\_acc}\right)^2 + \left(\frac{\partial \mathrm{EI(NO}x)}{\partial CO_2}\partial CO_{2\_bgr}\right)^2 + \\ &+\left(\frac{\partial \mathrm{EI(NO}x)}{\partial EI(CO_2)}\partial EI(CO_2)\right)^2 + \left(\frac{\partial \mathrm{EI(NO}x)}{\partial M(NO_2)}\partial M(NO_2)\right)^2 + \left(\frac{\partial \mathrm{EI(NO}x)}{\partial M(CO_2)}\partial M(CO_2)\right)^2\end{aligned}} \quad (3)$$

The individual uncertainty terms and the total EI uncertainty for EI(NO_x) are listed in Table 3. For EI(NO_x) the mean uncertainty from all in-flight plume encounters sums up to ~14%. Figure 8 further depicts the relative contribution of the individual terms to the total uncertainty for each plume encounter. It is evident that the most important uncertainty term for EI(NO_x) is the NO_y accuracy. For future aircraft campaigns we plan to implement a different dilution approach and suggest flying in a larger distance to the aircraft of interest to prevent the instrument from running into saturation effects.

Table 3: Individual contributions to total EI(NO_x) uncertainty for all in-flight exhaust encounters. The table denotes mean values; however the uncertainty is estimated for each individual plume encounter individually.

Uncertainty term for EI(NO_x)	Mean uncertainty estimate / %
∂NO_y acc	13
∂NO_y bgr	<1
∂CO_2 acc	<1
∂CO_2 bgr	1
∂EI(CO_2)	0.1
∂M(NO_2)	0.002
∂M(CO_2)	0.003
Total uncertainty ∂EI(NO_x)	14

The percentage contribution of the individual accuracy is generally higher (lower) when the encountered mixing ratio enhancement was low (high). The uncertainty of EI(CO_2), as well as of the molar masses, are negligible. The measurement uncertainties, i.e. the measurement accuracies for NO_y and CO_2 were described in the Materials and Method Section, including errors from the individual instruments, measurement techniques and calibration procedures. These absolute measurement accuracies (in ppb and ppm) are then translated into a relative accuracy (in %) based on the maximum mixing ratio enhancement observed during each exhaust plume encounter. The mean relative accuracy for CO_2 is <1% (0.1-2.5%) and for NO_y 13% (9-23%), see Table 3. The atmospheric background mole fraction needs to be determined for each individual plume encounter individually to account for horizontal, vertical as well as temporal gradients in the ambient atmosphere. However,

https://doi.org/10.5194/egusphere-2024-454
Preprint. Discussion started: 28 February 2024

the typical atmospheric background variation of NO_y (Δ4 ppb) and CO_2 (Δ5 ppm) is not sensitive to the high mixing ratios encountered (ΔNO_y ~500-4000 ppb, ΔCO_2 ~100-800ppm). The atmospheric background itself is estimated based on the following assumption. Primarily, prior to and after the plume encounter the probed air mass needs to be free of engine exhaust. Due to the natural dynamics of the troposphere, the atmospheric background for the long-lived gases CO_2 is not always as obvious as in the short-lived NO_y, hence, NO_y is taken as the main focus for this determination. If prior and after the encounter the mole fractions are identical, this value is taken for the atmospheric background. If the mole fractions are different, the atmospheric background is set in between these values. The mean difference from the mixing ratio at the start and end of the individual plume encounter to the respective atmospheric background estimate is considered in the uncertainty of the atmospheric background estimate. Moreover, the standard deviation (1σ) of an atmospheric background-like sequence is taken into account.

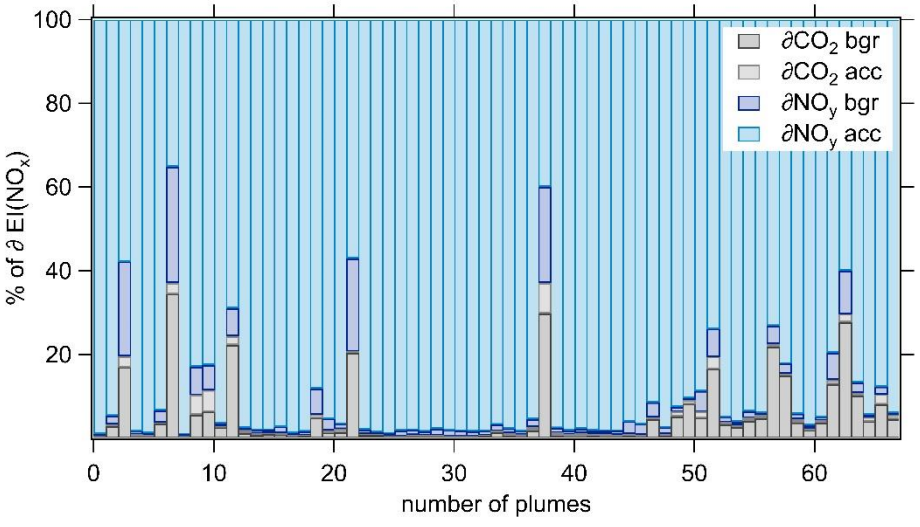

Figure 8: Stacked individual uncertainties for EI(NO_x) for in-flight plume encounters.

Conclusion

In conclusion, we presented the first EI(NO_x) in-flight measurements for a modern long-range aircraft and engines since 1995 (Schulte et al., 1997). We showed that the measurements and methodology are adequate to infer EI(NO_x) emissions from aircraft at high altitudes. As expected from previous ground engine tests, the fuel type, even a 100% SAF, has no statistically significant effect on the NO_x emission index. EI(NO_x) increases with increasing combustion temperature, pressure, and fuel flow for the measured cruise T3 range conditions. Furthermore, the in-flight in situ measurements generally agree with predictions from three different engine emission prediction methods within combined uncertainties when using data sets from the emission data base release as input, with a slight trend towards modelled lower emission indices. In order to take into account performance variations of the operational engines during maintenance cycles and to avoid engine to engine performance variations we performed ground measurements behind the same engine over a wide T3 range. The ground

https://doi.org/10.5194/egusphere-2024-454
Preprint. Discussion started: 28 February 2024

measurements show an increase in EI(NO_x) with increasing thrust, as explained by higher combustor temperatures. The ground measurements were then used as input to predict EI(NO_x) at cruise altitudes for typical cruise conditions using current engine models. The models generally agree better with the measured EI(NO_x) for in flight observations at typical cruise conditions with respect to P3, T3, AFR and Mach number. These campaigns present the first in-flight measurements targeting NO_x emissions of latest-generation engines at high altitudes and thus provide a valuable data set of EI(NO_x) cruise measurements for the evaluation of state-of-the art engine models. The observations thereby enhance the sparse existing data set of cruise emissions of older generation engines.

Data Availability

The CO_2 and NO_y flight measurement data are released at https://doi.org/10.5281/zenodo.10646359 (Harlass et al., 2024).

Author Contribution

TH analyzed the NO_y and CO2 measurement data and wrote the manuscript with inputs from all co-authors. TH, RD, RM, DS, MS, SK and PSt performed the Falcon measurements. TS, TG and LB performed the ground-based measurements. CV and CR concepted and designed the aircraft campaigns. US, MJ, DL, DA and PM performed the model simulations. All authors contributed to the interpretation of the data, reviewed the manuscript and have given approval to its final version.

Competing Interests

CR and MG are employed by Airbus Operations SAS; MJ, DL, PM and PSw are employed by Rolls-Royce plc. 725 and DA by Rolls-Royce Deutschland; RS is employed by Neste Corporation. All other authors declare that they have no conflict of interest.

Funding Sources

TB was funded by the Deutsche Forschungsgemeinschaft (DFG, German Research Foundation) under project nr 510826369 and CV by DFG SPP 1294 HALO under project nr VO1504_9 and by European Union under Grant Agreement No 101101999 and No 101114613.

Acknowledgments

The authors especially thank DLR-FX for the campaign cooperation. This involves not only our pilots Michael Grossrubatscher, Thomas von Marwick, Philipp Weber and Roland Welser, but also the management Georg Dietz and Oliver Paxa and the group of Martin Zöger, Andreas Giez, Vladyslav Nenakhov, Christoph Grad, Marina Schimpf, Christian Mallaun,

https://doi.org/10.5194/egusphere-2024-454
Preprint. Discussion started: 28 February 2024

David Woudsma, Alexander Wolf, Frank Probst, Stefan Hempe and many more. We also thank the flight test team of Airbus for the great coordination of the aircraft on ground as well as in the test areas. Great recognition is dedicated to the Rolls-Royce Technical Support team in Toulouse. And a special thanks is dedicated to all other ECLIF3 partners for their helpful cooperation. We would also like to thank Roger Teoh and Mark Stettler, who provided the source code for modelling emission indices.

References

Airbus: An A350 fuelled by 100% SAF just took off, 18 March 2021, https://www.airbus.com/en/newsroom/stories/2021-03-an-a350-fuelled-by-100-saf-just-took-off, last access 25.08.2023, 2021a.

Airbus: First in-flight 100% sustainable-fuels emissions study of passenger jet shows early promise, Toulouse, 29 November 2021, https://www.airbus.com/en/newsroom/press-releases/2021-11-first-in-flight-100-sustainable-fuels-emissions-study-of-passenger, last access 15.05.2023, 2021b.

Bollinger, M. J., Sievers, R. E., Fahey, D. W., and Fehsenfeld, F. C.: Conversion of nitrogen dioxide, nitric acid, and n-propyl nitrate to nitric oxide by a gold-catalyzed reduction with carbon monoxide, Analytical Chemistry, 55, 1980-1986, 10.1021/ac00262a034, 1983.

Bradshaw, J., Davis, D., Grodzinsky, G., Smyth, S., Newell, R., Sandholm, S., and Liu, S.: Observed distributions of nitrogen oxides in the remote free troposphere from the Nasa Global Tropospheric Experiment Programs, Reviews of Geophysics, 38, 61-116, https://doi.org/10.1029/1999RG900015, 2000.

Brasseur, G. P., Müller, J.-F., and Granier, C.: Atmospheric impact of NOx emissions by subsonic aircraft: A three-dimensional model study, Journal of Geophysical Research: Atmospheres, 101, 1423-1428, https://doi.org/10.1029/95JD02363, 1996.

Bräuer, T., Voigt, C., Sauer, D., Kaufmann, S., Hahn, V., Scheibe, M., Schlager, H., Huber, F., Le Clercq, P., Moore, R. H., and Anderson, B. E.: Reduced ice number concentrations in contrails from low-aromatic biofuel blends, Atmos. Chem. Phys., 21, 16817-16826, 10.5194/acp-21-16817-2021, 2021a.

Bräuer, T., Voigt, C., Sauer, D., Kaufmann, S., Hahn, V., Scheibe, M., Schlager, H., Diskin, G. S., Nowak, J. B., DiGangi, J. P., Huber, F., Moore, R. H., and Anderson, B. E.: Airborne Measurements of Contrail Ice Properties—Dependence on Temperature and Humidity, Geophysical Research Letters, 48, e2020GL092166, https://doi.org/10.1029/2020GL092166, 2021b.

Bulzan, D., Anderson, B., Wey, C., Howard, R., Winstead, E., Beyersdorf, A., Corporan, E., DeWitt, M. J., Klingshirn, C., Herndon, S., Miake-Lye, R., Timko, M., Wood, E., Tacina, K. M., Liscinsky, D., Hagen, D., Lobo, P., and Whitefield, P.: Gaseous and Particulate Emissions Results of the NASA Alternative Aviation Fuel Experiment (AAFEX), ASME Turbo Expo 2010: Power for Land, Sea, and Air, 1195-1207, 10.1115/gt2010-23524,

Dahlmann, K., Grewe, V., Ponater, M., and Matthes, S.: Quantifying the contributions of individual NOx sources to the trend in ozone radiative forcing, Atmospheric Environment, 45, 2860-2868, https://doi.org/10.1016/j.atmosenv.2011.02.071, 2011.

Deidewig, F., Döpelheuer, A., and Lecht, M.: Methods to assess aircraft engine emissions in flight, ICAS PROCEEDINGS, 131-141,

Döpelheuer, A. and Lecht, M.: Influence of engine performance on emission characteristics,

Drummond, J. W., Volz, A., and Ehhalt, D. H.: An optimized chemiluminescence detector for tropospheric NO measurements, Journal of Atmospheric Chemistry, 2, 287-306, 10.1007/BF00051078, 1985.

DuBois, D. and Paynter, G. C.: "Fuel Flow Method2" for Estimating Aircraft Emissions, https://doi.org/10.4271/2006-01-1987, 2006.

EEDB: ICAO Aircraft Engine Emissions Databank v28B, https://www.easa.europa.eu/en/domains/environment/icao-aircraft-engine-emissions-databank [dataset], 2021.

Fahey, D. W., Eubank, C. S., Hübler, G., and Fehsenfeld, F. C.: Evaluation of a catalytic reduction technique for the measurement of total reactive odd-nitrogen NOyin the atmosphere, Journal of Atmospheric Chemistry, 3, 435-468, 10.1007/BF00053871, 1985.

https://doi.org/10.5194/egusphere-2024-454
Preprint. Discussion started: 28 February 2024

Fiehn, A., Kostinek, J., Eckl, M., Klausner, T., Gałkowski, M., Chen, J., Gerbig, C., Röckmann, T., Maazallahi, H., Schmidt, M., Korbeń, P., Neçki, J., Jagoda, P., Wildmann, N., Mallaun, C., Bun, R., Nickl, A. L., Jöckel, P., Fix, A., and Roiger, A.: Estimating CH4, CO2 and CO emissions from coal mining and industrial activities in the Upper Silesian Coal Basin using an aircraft-based mass balance approach, Atmos. Chem. Phys., 20, 12675-12695, 10.5194/acp-20-12675-2020, 2020.

Gokulakrishnan, P. and Klassen, M. S.: NOx and CO Formation and Control, in: Gas Turbine Emissions, edited by: Lieuwen, T. C., and Yang, V., Cambridge Aerospace Series, Cambridge University Press, Cambridge, 175-208, DOI: 10.1017/CBO9781139015462.011, 2013.

Grewe, V., Matthes, S., and Dahlmann, K.: The contribution of aviation NOx emissions to climate change: are we ignoring methodological flaws?, Environmental Research Letters, 14, 121003, 10.1088/1748-9326/ab5dd7, 2019.

Harlass, T., Scheibe, M., and Roiger, A.: CO2 and NOy aircraft measurement data obtained within the framework of the ECLIF3 campaign [Data set]. Zenodo. https://doi.org/10.5281/zenodo.10646359 [dataset], 2024.

ICAO: Annex 16 to the Convention on International Civil Aviation, Environmental Protection, Volume II Aircraft Engine Emissions, Third Edition, July 2008, ISBN 978-92-9231-123-0, 2008.

ICAO: Airport Air Quality Manual, Doc 9889, Second Edition, ISBN 978-92-9258-963-9, 2020.

ICAO: ICAO Aircraft Engine Emissions Databank v29, February 2023, https://www.easa.europa.eu/en/domains/environment/icao-aircraft-engine-emissions-databank, last access 04.05.2023, 2023.

IPCC: IPCC, 1999 – J.E.Penner, D.H.Lister, D.J.Griggs, D.J.Dokken, M.McFarland (Eds.) Prepared in collaboration with the Scientific Assessment Panel to the Montreal Protocol on Substances that Deplete the Ozone Layer Cambridge University Press, UK. pp 373 Available from Cambridge University Press, The Edinburgh Building Shaftesbury Road, Cambridge CB2 2RU ENGLAND, 1999.

IPCC: Climate Change 2021: The Physical Science Basis. Contribution of Working Group I to the Sixth Assessment Report of the Intergovernmental Panel on Climate Change, Cambridge University Press, Cambridge, United Kingdom and New York, NY, USA, 10.1017/9781009157896, 2021.

Kärcher, B., Hirschberg, M. M., and Fabian, P.: Small-scale chemical evolution of aircraft exhaust species at cruising altitudes, Journal of Geophysical Research: Atmospheres, 101, 15169-15190, https://doi.org/10.1029/96JD01059, 1996.

Klausner, T., Mertens, M., Huntrieser, H., Galkowski, M., Kuhlmann, G., Baumann, R., Fiehn, A., Jöckel, P., Pühl, M., and Roiger, A.: Urban greenhouse gas emissions from the Berlin area: A case study using airborne CO2 and CH4 in situ observations in summer 2018, Elementa: Science of the Anthropocene, 8, 10.1525/elementa.411, 2020.

Klausner, T. M.: Aircraft-based in situ measurements of CH4 and CO2 downstream of European and Asian urban centres at local to synoptic scales, lmu, 2020.

Kleine, J., Voigt, C., Sauer, D., Schlager, H., Scheibe, M., Jurkat-Witschas, T., Kaufmann, S., Kärcher, B., and Anderson, B. E.: In Situ Observations of Ice Particle Losses in a Young Persistent Contrail, Geophysical Research Letters, 45, 13,553-513,561, https://doi.org/10.1029/2018GL079390, 2018.

Köhler, M. O., Rädel, G., Dessens, O., Shine, K. P., Rogers, H. L., Wild, O., and Pyle, J. A.: Impact of perturbations to nitrogen oxide emissions from global aviation, Journal of Geophysical Research: Atmospheres, 113, https://doi.org/10.1029/2007JD009140, 2008.

Lavoie, G. A., Heywood, J. B., and Keck, J. C.: Experimental and Theoretical Study of Nitric Oxide Formation in Internal Combustion Engines, Combustion Science and Technology, 1, 313-326, 10.1080/00102206908952211, 1970.

Le Quéré, C., Jackson, R. B., Jones, M. W., Smith, A. J. P., Abernethy, S., Andrew, R. M., De-Gol, A. J., Willis, D. R., Shan, Y., Canadell, J. G., Friedlingstein, P., Creutzig, F., and Peters, G. P.: Temporary reduction in daily global CO2 emissions during the COVID-19 forced confinement, Nature Climate Change, 10, 647-653, 10.1038/s41558-020-0797-x, 2020.

Lee, D. S., Pitari, G., Grewe, V., Gierens, K., Penner, J. E., Petzold, A., Prather, M. J., Schumann, U., Bais, A., Berntsen, T., Iachetti, D., Lim, L. L., and Sausen, R.: Transport impacts on atmosphere and climate: Aviation, Atmospheric Environment, 44, 4678-4734, https://doi.org/10.1016/j.atmosenv.2009.06.005, 2010.

Lee, D. S., Fahey, D. W., Skowron, A., Allen, M. R., Burkhardt, U., Chen, Q., Doherty, S. J., Freeman, S., Forster, P. M., Fuglestvedt, J., Gettelman, A., De León, R. R., Lim, L. L., Lund, M. T., Millar, R. J., Owen, B., Penner, J. E., Pitari, G., Prather, M. J., Sausen, R., and Wilcox, L. J.: The contribution of global aviation to anthropogenic climate forcing for 2000 to 2018, https://doi.org/10.1016/j.atmosenv.2020.117834, 2021/01/01/.

LI-COR: The Importance of Water VaporMeasurements and Corrections, Tech Tip, 2003.

LI-COR: Li-7000 CO2/H2O Analyzer, Instruction Manual, Publication Number 984-07364, 2007.

https://doi.org/10.5194/egusphere-2024-454
Preprint. Discussion started: 28 February 2024

Märkl, R. S., Voigt, C., Sauer, D., Dischl, R. K., Kaufmann, S., Harlaß, T., Hahn, V., Roiger, A., Weiß-Rehm, C., Burkhardt, U., Schumann, U., Marsing, A., Scheibe, M., Dörnbrack, A., Renard, C., Gauthier, M., Swann, P., Madden, P., Luff, D., Sallinen, R., Schripp, T., and Le Clercq, P.: Powering aircraft with 100% sustainable aviation fuel reduces ice crystals in contrails, EGUsphere, 2023, 1-37, 10.5194/egusphere-2023-2638, 2023.

Moore, R. H., Thornhill, K. L., Weinzierl, B., Sauer, D., D'Ascoli, E., Kim, J., Lichtenstern, M., Scheibe, M., Beaton, B., Beyersdorf, A. J., Barrick, J., Bulzan, D., Corr, C. A., Crosbie, E., Jurkat, T., Martin, R., Riddick, D., Shook, M., Slover, G., Voigt, C., White, R., Winstead, E., Yasky, R., Ziemba, L. D., Brown, A., Schlager, H., and Anderson, B. E.: Biofuel blending reduces particle emissions from aircraft engines at cruise conditions, Nature, 543, 411-415, 10.1038/nature21420, 2017.

Norman, P., Lister, D., Lecht, M., Madden, P., Park, K., Penanhoat, O., Plaisance, C., and Renger, K.: Development of the Technical Basis for a New Emissions Parameter Covering the Whole AIRcraft Operation: NEPAIR-Final Technical Report; European Commission Project, Report No. GRD1-1999-10439., 2003.

Ridley, B. A. and Howlett, L. C.: An instrument for nitric oxide measurements in the stratosphere, Review of Scientific Instruments, 45, 742-746, 10.1063/1.1686726, 1974.

Roiger, A., Thomas, J. L., Schlager, H., Law, K. S., Kim, J., Schäfler, A., Weinzierl, B., Dahlkötter, F., Krisch, I., Marelle, L., Minikin, A., Raut, J. C., Reiter, A., Rose, M., Scheibe, M., Stock, P., Baumann, R., Bouarar, I., Clerbaux, C., George, M., Onishi, T., and Flemming, J.: Quantifying Emerging Local Anthropogenic Emissions in the Arctic Region: The ACCESS Aircraft Campaign Experiment, Bulletin of the American Meteorological Society, 96, 441-460, https://doi.org/10.1175/BAMS-D-13-00169.1, 2015.

Rolls-Royce: Aviation leaders launch first in-flight 100% sustainable-fuel emissions study on commercial passenger jet, 18 March 2021, https://www.rolls-royce.com/media/press-releases/2021/18-03-2021-aviation-leaders-launch-first-in-flight-100-percent-sustainable-fuel-emissions.aspx, last access 25.08.2023, 2021.

SAE: SAE Aerospace Information Report, 2009, "AIR5715 Procedure for the Calculation of Aircraft Emissions," SAE International, Warrendale, PA, Report, 2009.

Schaefer, M. and Bartosch, S.: Overview on fuel flow correlation methods for the calculation of NOx, CO and HC emissions and their implementation into aircraft performance software, 2013.

Schlager, H., Konopka, P., Schulte, P., Schumann, U., Ziereis, H., Arnold, F., Klemm, M., Hagen, D. E., Whitefield, P. D., and Ovarlez, J.: In situ observations of air traffic emission signatures in the North Atlantic flight corridor, Journal of Geophysical Research: Atmospheres, 102, 10739-10750, https://doi.org/10.1029/96JD03748, 1997.

Schmitt, J.: Aufbau und Erprobung eines in-situ NO/NOy-Mess-Systems am Höhenforschungsflugzeug M55-Geophysica, Dissertation, LMU München, 2003.

Schripp, T., Anderson, B. E., Bauder, U., Rauch, B., Corbin, J. C., Smallwood, G. J., Lobo, P., Crosbie, E. C., Shook, M. A., Miake-Lye, R. C., Yu, Z., Freedman, A., Whitefield, P. D., Robinson, C. E., Achterberg, S. L., Köhler, M., Oßwald, P., Grein, T., Sauer, D., Voigt, C., Schlager, H., and LeClercq, P.: Aircraft engine particulate matter emissions from sustainable aviation fuels: Results from ground-based measurements during the NASA/DLR campaign ECLIF2/ND-MAX, Fuel, 325, 124764, https://doi.org/10.1016/j.fuel.2022.124764, 2022.

Schulte, P. and Schlager, H.: In-flight measurements of cruise altitude nitric oxide emission indices of commercial jet aircraft, Geophysical Research Letters, 23, 165-168, https://doi.org/10.1029/95GL03691, 1996.

Schulte, P., Schlager, H., Ziereis, H., Schumann, U., Baughcum, S. L., and Deidewig, F.: NO x emission indices of subsonic long-range jet aircraft at cruise altitude: In situ measurements and predictions, Journal of Geophysical Research: Atmospheres, 102, 21431-21442, https://doi.org/10.1029/97JD01526, 1997.

Schumann, U., Poll, I., Teoh, R., Koelle, R., Spinielli, E., Molloy, J., Koudis, G., Baumann, R., Bugliaro, L., Stettler, M., and Voigt, C.: Air traffic and contrail changes over Europe during COVID-19: A model study, Atmospheric Chemistry and Physics, 21, 7429-7450, 10.5194/acp-21-7429-2021, 2021.

Skowron, A., Lee, D. S., De León, R. R., Lim, L. L., and Owen, B.: Greater fuel efficiency is potentially preferable to reducing NOx emissions for aviation's climate impacts, Nature Communications, 12, 564, 10.1038/s41467-020-20771-3, 2021.

Stratmann, G.: Stickoxidmessungen in der Tropopausenregion an Bord eines Linienflugzeugs: Großräumige Verteilung und Einfluss des Luftverkehrs, 2013.

Stratmann, G., Ziereis, H., Stock, P., Brenninkmeijer, C. A. M., Zahn, A., Rauthe-Schöch, A., Velthoven, P. V., Schlager, H., and Volz-Thomas, A.: NO and NOy in the upper troposphere: Nine years of CARIBIC measurements onboard a passenger aircraft, Atmospheric Environment, 133, 93-111, https://doi.org/10.1016/j.atmosenv.2016.02.035, 2016.

https://doi.org/10.5194/egusphere-2024-454
Preprint. Discussion started: 28 February 2024

Teoh, R., Schumann, U., Gryspeerdt, E., Shapiro, M., Molloy, J., Koudis, G., Voigt, C., and Stettler, M. E. J.: Aviation contrail climate effects in the North Atlantic from 2016 to 2021, Atmos. Chem. Phys., 22, 10919-10935, 10.5194/acp-22-10919-2022, 2022.

Terrenoire, E., Hauglustaine, D. A., Cohen, Y., Cozic, A., Valorso, R., Lefèvre, F., and Matthes, S.: Impact of present and future aircraft NOx and aerosol emissions on atmospheric composition and associated direct radiative forcing of climate, Atmos. Chem. Phys., 22, 11987-12023, 10.5194/acp-22-11987-2022, 2022.

Tremmel, H. G., Schlager, H., Konopka, P., Schulte, P., Arnold, F., Klemm, M., and Droste-Franke, B.: Observations and model calculations of jet aircraft exhaust products at cruise altitude and inferred initial OH emissions, Journal of Geophysical Research: Atmospheres, 103, 10803-10816, https://doi.org/10.1029/97JD03451, 1998.

Voigt, C., Jurkat, T., Schlager, H., Schäuble, D., Petzold, A., and Schumann, U.: Aircraft Emissions at Cruise and Plume Processes, in: Atmospheric Physics: Background – Methods – Trends, edited by: Schumann, U., Springer Berlin Heidelberg, Berlin, Heidelberg, 675-692, 10.1007/978-3-642-30183-4_41, 2012.

Voigt, C., Schumann, U., Jessberger, P., Jurkat, T., Petzold, A., Gayet, J.-F., Krämer, M., Thornberry, T., and Fahey, D. W.: Extinction and optical depth of contrails, Geophysical Research Letters, 38, https://doi.org/10.1029/2011GL047189, 2011.

Voigt, C., Kleine, J., Sauer, D., Moore, R. H., Bräuer, T., Le Clercq, P., Kaufmann, S., Scheibe, M., Jurkat-Witschas, T., Aigner, M., Bauder, U., Boose, Y., Borrmann, S., Crosbie, E., Diskin, G. S., DiGangi, J., Hahn, V., Heckl, C., Huber, F., Nowak, J. B., Rapp, M., Rauch, B., Robinson, C., Schripp, T., Shook, M., Winstead, E., Ziemba, L., Schlager, H., and Anderson, B. E.: Cleaner burning aviation fuels can reduce contrail cloudiness, Communications Earth & Environment, 2, 114, 10.1038/s43247-021-00174-y, 2021.

Voigt, C., Lelieveld, J., Schlager, H., Schneider, J., Curtius, J., Meerkötter, R., Sauer, D., Bugliaro, L., Bohn, B., Crowley, J. N., Erbertseder, T., Groß, S., Hahn, V., Li, Q., Mertens, M., Pöhlker, M. L., Pozzer, A., Schumann, U., Tomsche, L., Williams, J., Zahn, A., Andreae, M., Borrmann, S., Bräuer, T., Dörich, R., Dörnbrack, A., Edtbauer, A., Ernle, L., Fischer, H., Giez, A., Granzin, M., Grewe, V., Harder, H., Heinritzi, M., Holanda, B. A., Jöckel, P., Kaiser, K., Krüger, O. O., Lucke, J., Marsing, A., Martin, A., Matthes, S., Pöhlker, C., Pöschl, U., Reifenberg, S., Ringsdorf, A., Scheibe, M., Tadic, I., Zauner-Wieczorek, M., Henke, R., and Rapp, M.: Cleaner Skies during the COVID-19 Lockdown, Bulletin of the American Meteorological Society, 103, E1796-E1827, https://doi.org/10.1175/BAMS-D-21-0012.1, 2022.

Wormhoudt, J., Herndon, S. C., Yelvington, P. E., Miake-Lye, R. C., and Wey, C.: Nitrogen Oxide (NO/NO2/HONO) Emissions Measurements in Aircraft Exhausts, Journal of Propulsion and Power, 23, 906-911, 10.2514/1.23461, 2007.

Ziereis, H., Schlager, H., Schulte, P., van Velthoven, P. F. J., and Slemr, F.: Distributions of NO, NO x , and NO y in the upper troposphere and lower stratosphere between 28° and 61°N during POLINAT 2, Journal of Geophysical Research: Atmospheres, 105, 3653-3664, https://doi.org/10.1029/1999JD900870, 2000.

Ziereis, H., Hoor, P., Grooß, J. U., Zahn, A., Stratmann, G., Stock, P., Lichtenstern, M., Krause, J., Bense, V., Afchine, A., Rolf, C., Woiwode, W., Braun, M., Ungermann, J., Marsing, A., Voigt, C., Engel, A., Sinnhuber, B. M., and Oelhaf, H.: Redistribution of total reactive nitrogen in the lowermost Arctic stratosphere during the cold winter 2015/2016, Atmos. Chem. Phys., 22, 3631-3654, 10.5194/acp-22-3631-2022, 2022.